J MATER SCI 41 (2006) 2201–2209

Sol-gel elaboration and characterization of YAG: Tb^{3+} powdered phosphors

A. POTDEVIN, G. CHADEYRON*, D. BOYER, R. MAHIOU
Laboratoire des Matériaux Inorganiques, Université Blaise Pascal and ENSCCF, 24 Avenue des Landais, 63177, Aubière Cedex, France
E-mail: chadeyr@chimpt.uiv-bpclermont.fr

Published online: 9 March 2006

Pure and Tb^{3+}-doped $Y_3Al_5O_{12}$ materials have been successfully synthesized from sol-gel based alkoxide precursors. Their formation process, structure and microstructure were examined by means of X-ray diffraction (XRD), thermal analysis combined with infrared spectroscopy (TG-IR / TDA), infrared spectroscopy (IR), scanning electron microscopy (SEM) and solid-state NMR study (^{27}Al MAS NMR). Pure highly crystalline YAG powders were obtained from 900°C. Laser induced luminescence spectra as well as decay times versus Tb^{3+} concentration were also studied. The well known $^5D_3 \rightarrow {}^5D_4$ cross-relaxation and concentration quenching phenomena were observed. Decay times of the green emission ($\lambda_{em} = 544$ nm) were mainly found to be exponential with time constant lower than 5 ms. Finally, the optimal terbium concentration for the luminescence efficiency of YAG:Tb^{3+} powders was determined.

1. Introduction

Rare-earth doped $Y_3Al_5O_{12}$ (YAG) materials are currently attracting attention due to their high luminescence efficiency under several types of radiations. Besides, with activators such as Nd, Sm, Eu, Ce and Gd, yttrium aluminum garnet matrix shows emissions which spread from the near infra-red range to the UV range of the electromagnetic spectrum. Furthermore, YAG presents an important damage threshold, leading it to withstand harsh conditions.

Such peculiarities have suggested the use of this material as radiation densimeter, scintillator, as well as phosphor for a new generation of television screens (field emission display—FED, plasma display panels—PDP, electroluminescent devices—ELD, . . .) and a new generation of free Hg lamps [1–8].

Since numerous of these applications need materials in shape of films or powders with a high degree of purity, several synthesis routes have been investigated based essentially on solid-state reaction [1, 3, 9]. However, theses processes require constraining annealing procedures to obtain pure phases. Therefore, a simple and economical method for making high quality materials is desirable. Several soft chemical processes have been developped for such purpose, including co-precipitation [10–12], spray pyrolysis [13], hydrothermal synthesis [14, 15], sol-gel [7, 16] or citrate-nitrate gel combustion [17–19].

Among these methods, the sol-gel route is one of the most important since it presents a lot of advantages : low-temperature synthesis, possible formation of powders with uniform grain morphology and achievement of homogeneous multicomponent films. Such technique has been succesfully used to obtain undoped [16, 20–26] and rare-eath activated YAG phosphors [7, 26–32].

YAG:Tb^{3+} has been studied extensively due to its well-known green emission which can be efficiently sensitized by means of several sources such as cathode-ray, VUV, UV and low-voltage excitations. In what follows, we describe the obtention of YAG and Tb^{3+}-doped YAG powders using an alkoxide route [28, 29]. Their crystallization temperature, phase evolution and morphology were investigated by X-ray diffraction (XRD), infrared spectroscopy (IR), infrared-spectroscopy combined to thermal analysis (DTA/ TG-IR) and scanning electron microscopy (SEM). In addition, ^{27}Al solid-state NMR spectra were recorded to characterize the local environment. Photoluminescence properties were evaluated through UV and blue excitations.

*Author to whom all correspondence should be addressed.

0022-2461
DOI: 10.1007/s10853-006-7182-7

2. Experimental procedure

2.1. Modus operandi

$Y_3Al_5O_{12}$ and terbium activated $Y_3Al_5O_{12}$ powders were prepared by hydrolysis, condensation and gelation of aluminum isopropoxide mixed with yttrium and terbium chlorides in isopropanol. This procedure is close to those used by Yamaguchi *et al*. [24, 25] and Ravichandran *et al*. [7].

It was necessary to work under anhydrous conditions in a dry argon atmosphere since moisture can harm considerably alkoxide stability. The first step consisted in the synthesis of yttrium and terbium alkoxide: anhydrous yttrium chloride YCl^3 ((3-*x*) eq., 99.99% pure, Aldrich) and anhydrous terbium chloride $TbCl^3$ (x eq., 99.99% pure, Aldrich) were dissolved in anhydrous isopropanol $^{i}PrOH$ (Acros Organics) under vigorous stirring for about 45 min (solution A). Meanwhile, chunks of metallic potassium (9 eq.) (Aldrich) were carefully cleaned by removing a superficial crust and then were dissolved in isopropanol under stirring (solution B).

Subsequently to complete dissolution, solution B was added with care to solution A with energetic stirring. We observed an exothermic reaction and KCl precipitated immediately. After 1 h reflux at 85°C, a known weight (5 eq.) of aluminum isopropoxide powder $Al(O^iPr)_3$ (Aldrich) was added directly to the solution. Under further reflux for 4 h at 85°C, a clear solution of yttrium terbium aluminum isopropoxide and a precipitate of potassium chloride were produced.

After cooling, this latter was eliminated by centrifugation and a clear sol was collected. Afterwards the sol was hydrolyzed by introducing an excess of water, resulting in transparent gel which was further dried at 80°C to yield a white xerogel. Undoped $Y_3Al_5O_{12}$ and $Y_3(1\text{-}x)Al_5O_{12}$: Tb_{3x} with *x* lying from 0.003 (0.1 mol.%) to 0.9 (30 mol.%) were prepared by this way.

2.2. Characterization techniques

XRD measurements were performed on a Philips Xpert Pro diffractometer operating with the Cu-K_α radiation. High temperature X-ray diffraction (HTXRD) analyses were carried out on the same diffractometer equipped with a high temperature chamber, over a temperature range lying from 25 to 1200°C in air atmosphere. A sequential temperature rising rate of $10°C{\cdot}min^{-1}$ and 1 h temperature holding time prior to measurement were used. Temperature was determined by means of Pt/ Pt-Rd thermocouple in direct contact with the powdered sample deposited onto a Pt ribbon.

The infrared spectra were recorded on a Perkin Elmer 2000 FTIR spectrometer using the KBr pellet technique.

Thermal analyses combined with infrared spectroscopy were undertaken on a Mettler Toledo TGA/SDTA851e under a $35\ ml{\cdot}min^{-1}$ O_2 flux: gas emitted were checked by IR analysis on a NEXUS Thermo Nicolet while samples were heated from room temperature to 1200°C at a rate of 10°C/min.

Micrographs were recorded by means of a Cambridge Scan-360 microscope operating at 20 kV. Specimens were prepared by sprinkling a small amount of powder on the surface of an adhesive carbon film. Then, a 20 nm Au coating was sputtered onto the surface.

^{27}Al NMR study was performed on a Bruker 300 spectrometer at 78.20 MHz. Magic angle spinning (MAS) at 10 kHz was used and a 4 mm diameter size zirconia rotor was employed as samples chamber. Peaks positions were referenced to external aqueous $AlCl_3$. Measurements were carried out under short radio frequency pulses associated with a recycling time of 500 ms. Chemical shifts are not corrected from the second order quadrupolar effect which induces their transference to lower frequencies.

The luminescence spectra were recorded with a monochromator Jobin-Yvon HR 1000 spectrometer, using a dye laser (continuum ND62) pumped by a frequency doubled pulsed YAG:Nd^{3+} laser (continuum surelite I). The dye solution was prepared by mixing Rhodamines 610 and 640. To achieve a resonant pumping in the blue wavelength range, the output of the dye laser was upshifted to 4155 cm^{-1} by stimulated Raman scattering in a high pressure gaseous H_2 cell [33]. Fluorescence decays were measured with a LeCroy 400 MHz digital oscilloscope.

3. Results and discussion

3.1. Powder X-ray diffraction

First of all, undoped compounds crystallization was analysed by means of HTXRD. The resulting patterns (Fig. 1) reveal that the xerogel remains amorphous until 850°C, since only the diffraction peaks of the platinum rod used as sample holder are observed up to that sintering temperature. Afterwards, the crystallization process occurs and becomes much more significant at high temperature since diffraction peaks are much sharper and well defined. After cooling (25°C, final), no more change is noticed and all the diffraction peaks can be assigned to the YAG structure (JCPDS-file 33-0040).

On the basis of this study, a 4h heat-treatment at 1100°C was chosen to anneal all the samples since it corresponds to the best conditions so as to provide suitable-crystallized YAG to perform optical analyses. The related XRD patterns for various terbium concentrations, gathered in Fig. 2, exhibit a single crystallized phase consistent with YAG compound unlike Mc Kittrick *et al*. [20] who reported the presence of unreacted Y_2O_3 and θ-Al_2O_3.

YAG ant TAG ($Tb_3Al_5O_{12}$) crystallize with the same garnet structure and additionnally Y^{3+} and Tb^{3+} ionic radii are very close ($r_Y{}^{3+} = 1.02$ and $r_{Tb}{}^{3+} = 1.04$ in coordination VIII). Consequently, XRD patterns are not strongly affected and show slightly shifted diffraction peaks even for the 30% Tb doped sample.

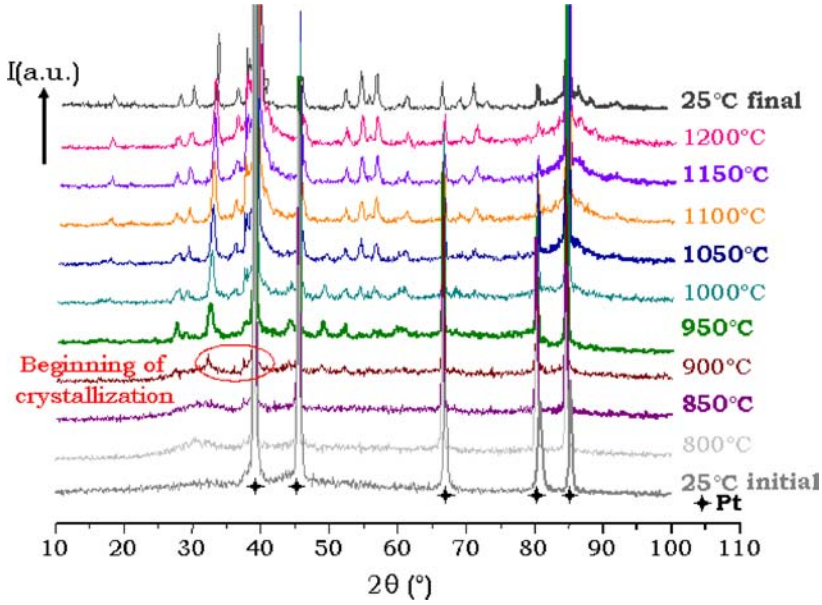

Figure 1 High temperature XRD patterns of undoped YAG.

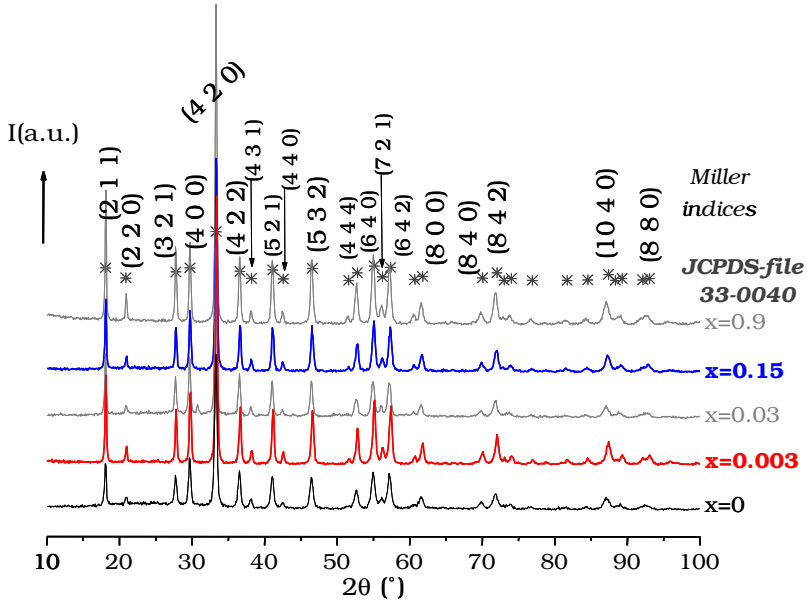

Figure 2 XRD patterns recorded for $Y_{3-x}Al_5O_{12}$:Tb_x samples for different terbium amounts.

3.2. Thermal behaviour

In order to study the thermal decomposition of undoped xerogels, thermal gravimetry analysis (TGA) combined with infrared (IR) spectroscopy were used.

TG and DTA results are presented in Fig. 3 [26, 28]. Fig. 4 shows cinetics of emitted gases during TG analysis, determined through the intensity evolution of the infrared main characteristic bands of each species. The total weight loss remains between -35 and -40% whatever the Tb^{3+} concentration is and occurs in three steps as shown in Fig. 3. The first one (25–200°C) corresponds to the departure of adsorbed moisture and chemically bonded alcohol molecules, in agreement with Fig. 4. This stage leads to a wide endothermic peak.

The second and main weight loss (−19%) lying from 200 to 600°C is associated with an exothermic phenomenon. This stage can be assigned to the pyrolysis of the organic parts of the alkoxide groups and likely to more strongly adsorbed alcohol molecules. It is in good agreement with IR measurements which show that most of the residual organic groups are removed before 600°C.

Above 600°C, only a weak weight loss takes place, ascribed to the withdrawal of the last residual alkoxy groups embedded in YAG matrix. Furthermore, a sharp exothermic peak at about 894°C indicates the onset of YAG crystallization [26, 28, 34–35]. This is consistent with the XRD results which showed that YAG sample begins to crystallize between 850 and 900°C. No significant weight

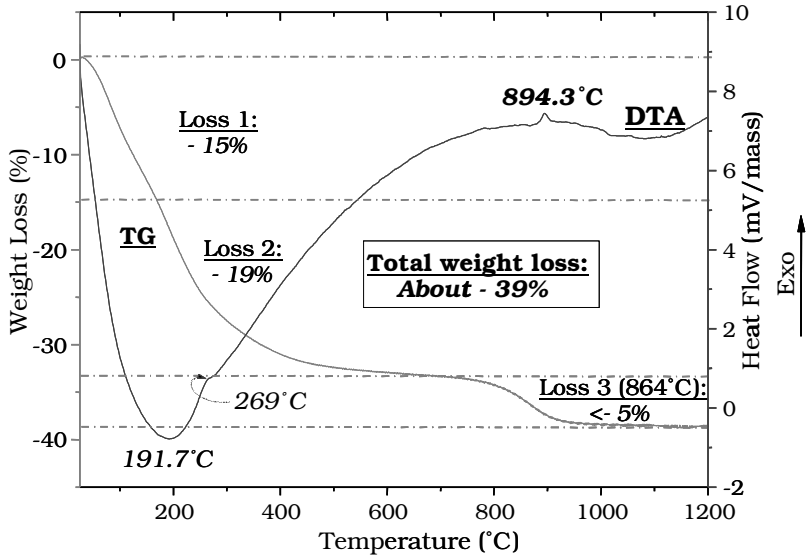

Figure 3 TG and DTA profiles obtained from YAG precursor gel.

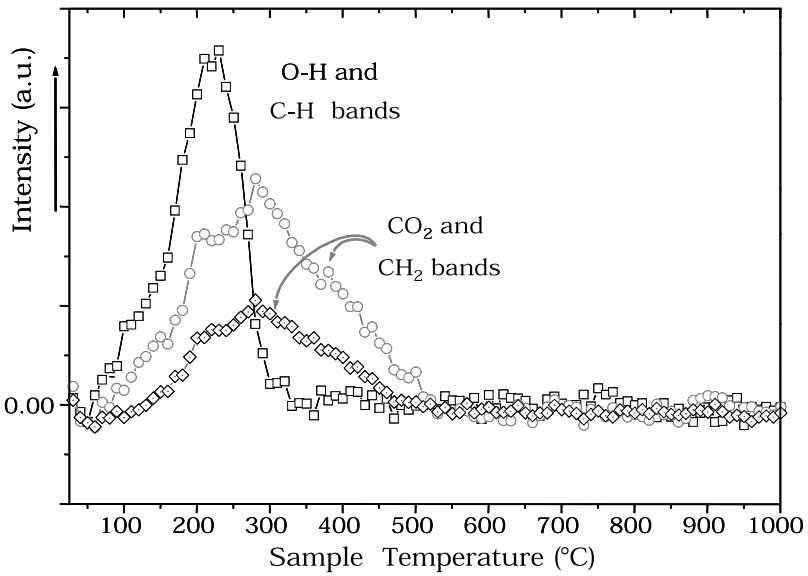

Figure 4 Cinetics of gases emitted during TG analysis.

loss appears thereafter, assuming the formation of the final product $Y_3Al_5O_{12}$.

3.3. Infrared spectroscopy

Fig. 5 shows the FTIR spectra of xerogel and undoped YAG sintered for 4 h at 1100°C. In the xerogel spectrum (Fig. 5a), the presence of the characteristic organic bands is noticed [26, 28]. The broad band ranging from 2600 cm^{-1} to 3800 cm^{-1} is ascribed to $^{-}CH_3$ and ^{-}OH stretching in the isopropanol and alkoxy groups. This latter also involves ^{-}OH stretching resulting from water added in excess for hydrolysis and adsorbed from air moisture. A peak of weak intensity at about 2350 cm^{-1} is attributed to the adsorbed carbon dioxide from the atmosphere. The bands lying from 1200 to 1600 cm^{-1} are attributed to C-O and -CH_3 stretches bonds of organic groups whereas the peaks at about 1638 cm^{-1} is likely due to water added in excess to hydrolyze the heterometallic isopropoxide sol. Moreover, the several broad bands observed whithin the 400–850 cm^{-1} region of the IR spectrum correspond to M-O bonds (M=Y or Al) vibrations in YAG lattice [28].

After sintering (Fig. 5b), specific bands related to the solvent and alkoxy groups significantly decrease or disappear. The carbon dioxide peak remains. Specific Al-O and Y-O vibrations peaks below 800 cm^{-1} are clearly identified as YAG ones [36, 37].

3.4. Scanning electron microscopy

It is known that luminescent properties of a phosphor depend on its particles shape and size [13]. On this account, the morphology of Tb^{3+}-activated YAG samples has been studied by scanning electron microscopy (SEM).

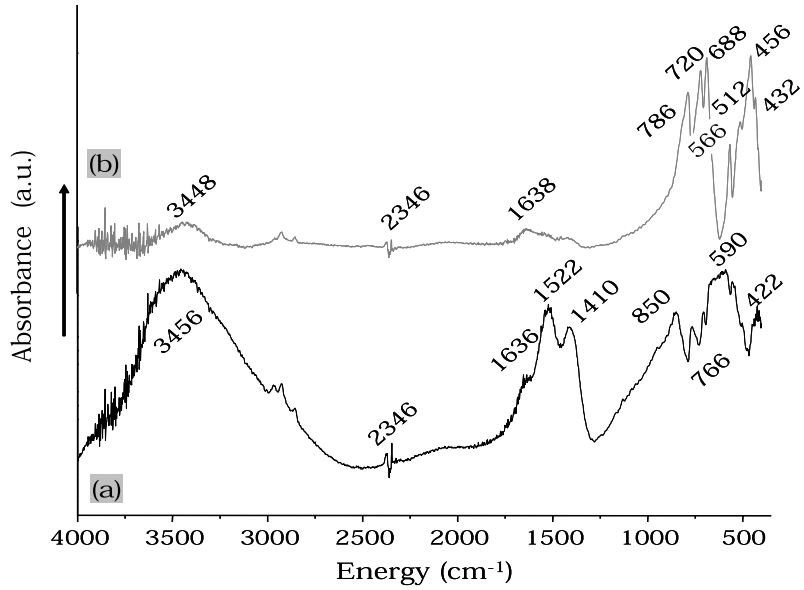

Figure 5 IR spectra of: (a) undoped dried gel precursor and (b) undoped YAG sintered at 1100°C for 4 h.

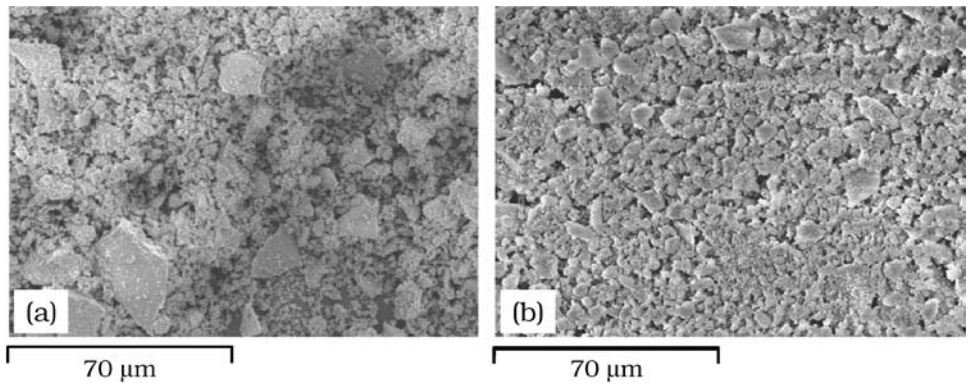

Figure 6 SEM images recorded at 800× magnification from $Y_3Al_5O_{12}:Tb^{3+}$(5%) unheated (a) and annealed at 1100°C for 4 h (b).

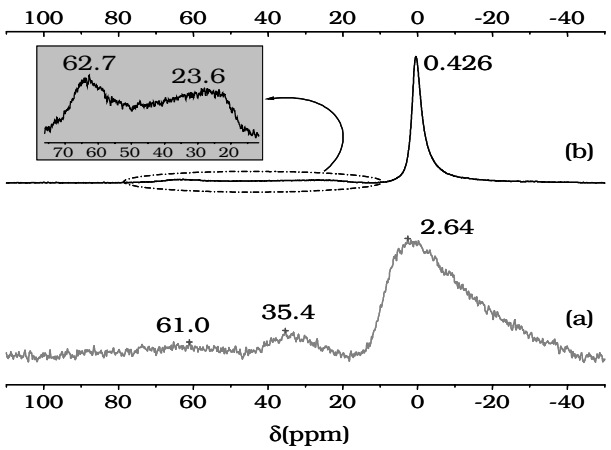

Figure 7 ^{27}Al MAS NMR spectra of YAG precursor gel (a) and powder annealed at 1100°C for 4 h (b).

SEM micrographs of YAG:Tb^{3+}(5%) powder recorded at 800× magnification are shown in Fig. 6. From the first picture related to the as-prepared xerogel (Fig. 6a), it can be seen irregular size blocks. Voids and pores are also observed. The micrograph of heat-treated sample (Fig. 6b) exhibits a denser network with fewer voids and narrow size distribution. For the two samples, the largest particles can reach several tens of micrometers.

3.5. NMR ^{27}Al

$Y_3Al_5O_{12}$ generally adopts a cubic garnet structure with lattice parameter of 12 Å(space group $Ia\bar{3}d$) [38]. Its structure consists of a network where aluminum atoms reside both in octahedral and tetrahedral interstices whereas yttrium atoms occupy dodecahedral sites [26, 38]. Since the chemical shift of ^{27}Al NMR is sensitive to the local coordination, this technique is largely applied for checking the different phases and coordination states of Al centers in aluminates [26, 35, 38]. As a result, MAS NMR ^{27}Al study has been undertaken on YAG samples in order to apprehend what kind of interatomic movements occur during sol-gel process.

Fig. 7 shows the ^{27}Al NMR spectra of undoped YAG samples before (a) and after (b) heat-treatment. According to several studies [39, 40 e.g.], chemical shifts of different coordination states of Al atoms are well

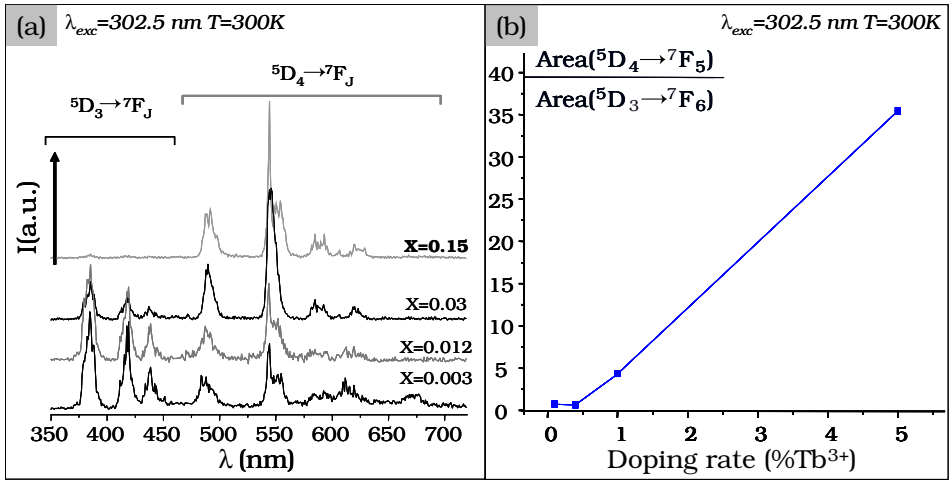

Figure 8 Room temperature (a) emission spectra of $Y_{3-x}Al_5O_{12}:Tb_x$ for different terbium concentrations and (b) study of $^5D_4 \rightarrow {}^7F_5$ and $^5D_3 \rightarrow {}^7F_6$ transition ratio as a function of doping rate—upon UV excitation.

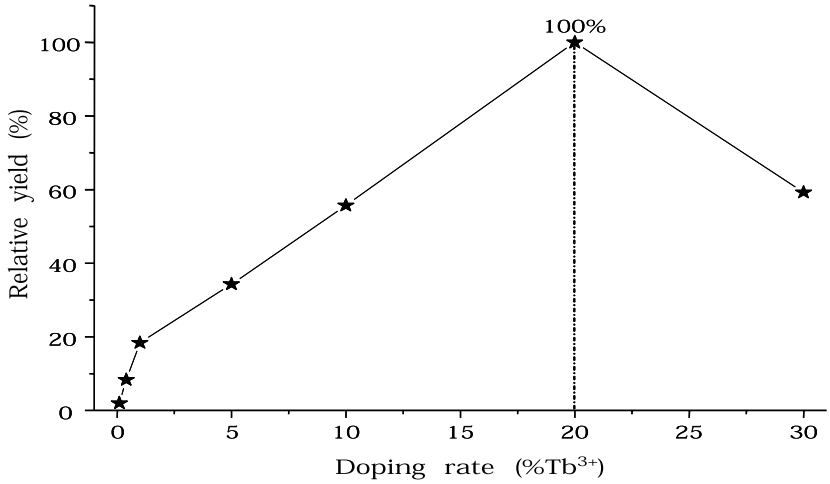

Figure 9 Concentration dependence of Tb^{3+} $^5D_4$ emission intensity after YAG:Nd^{3+} 485 nm excitation.

recognizable: octahedral AlO_6 sites resonate between 15 and −30 ppm, the much less common AlO_5 sites between 40 and 25 ppm and tetrahedral AlO_4 between 80 and 50 ppm. On this account, the 2.6 ppm major resonance in the spectrum of the uncalcined xerogel (Fig. 7a) corresponds to six-coordinate aluminum. Besides, two other distinct peaks located at about 35.4 and 61 ppm can be assigned to five and four-fold coordinated aluminum atoms. It can be noticed that the resonance at 35.4 ppm can also be consistent with a tetrahedral site distorted due to the presence of oxygen defects [35, 39].

^{27}Al NMR spectral features of the sintered YAG powder (Fig. 7b) reveal three signals at 0.426, 23.6 and 62.7 ppm, which can be imputed to the three types of coordination. The octahedral band has shrinked into the sharp signal at 0.426 ppm. Furthermore, since it has been demonstrated that Al atoms can only occupy tetrahedral and octahedral sites in crystallized YAG [26, 38], we can deduce that the 35.4 and 23.6 ppm signals respectively in xerogel and crystallized powder correspond to distorted tetrahedral site and not to five-fold coordinated one.

Besides, by integrating peak areas, the ^{27}Al tetrahedral/octahedral ratio has been determined. Contrary to other studies, such as McKenzie and Kemmitt's one [35], it remains the same after calcination, even if the resonance relative to "distorted tetrahedral" sites has weakened in favour of tetrahedral one.

3.6. Optical properties of YAG:Tb^{3+}

The photoluminescence of the YAG:Tb^{3+} annealed powders was recorded at room temperature for several terbium concentrations. Emission spectra recorded upon UV excitation are shown in Fig. 8a The spectral distribution is greatly dependent on terbium amount, which is consistent with other investigations [31, 32, 41, 42] in regards with different kinds of YAG:Tb^{3+} specimens (monocrystals, powders and films). Indeed, for the lowest concentrations of Tb^{3+}, spectra can readily be divided into two groups of lines: the blue emission below 480 nm is related to $^5D_3 \rightarrow {}^7FJ$ transitions whereas the green emission arises from $^5D_4 \rightarrow {}^7F_J$ (J=6 to 0) transitions [42–45]. As the terbium concentration increases, the blue emission

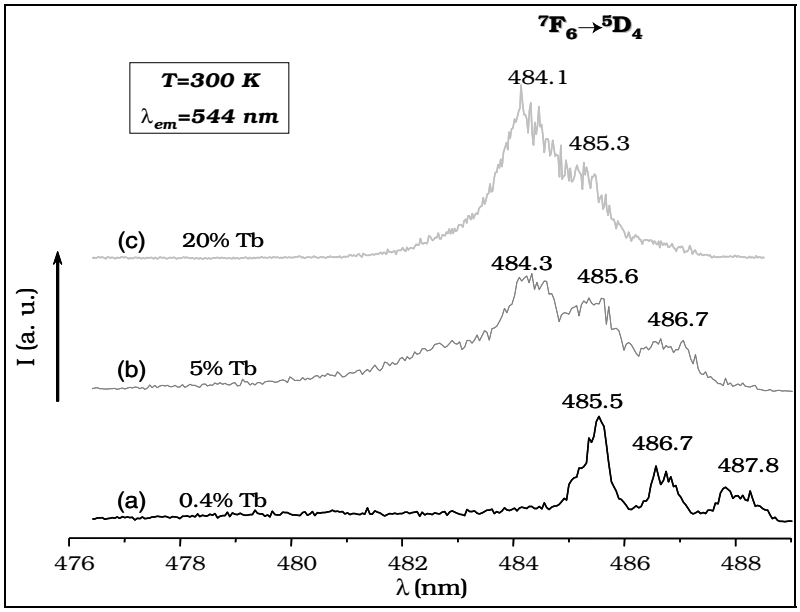

Figure 10 Room temperature excitation spectra of the $^5D_4 \rightarrow {}^7F_5$ in $Y_3Al_5O_{12}:Tb^{3+}$ (0.4%) (a) $Y_3Al_5O_{12}:Tb^{3+}$(5%) (b) and $Y_3Al_5O_{12}:Tb^{3+}$ (20%) (c).

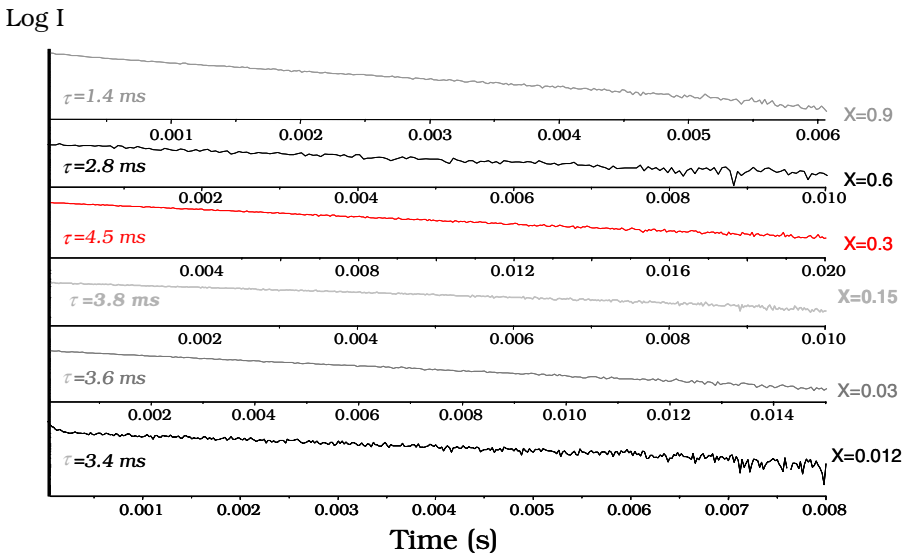

Figure 11 Luminescence decay curves of the $^5D_4 \rightarrow {}^7F_5$ emission of Tb^{3+} in $Y_3Al_5O_{12}:Tb^{3+}$ for different terbium concentrations at 300 K upon $^5D_4$ excitation.

weakens then dissappears: from $x = 0.15$ (5% Tb^{3+}), only $^5D_4 \rightarrow {}^7F_J$ transitions are recorded. Such observation corresponds to the well-known cross relaxation phenomenon [41–42] which can be illustrated by the following equation [46]:

$$Tb^{3+}(^5D_3) + Tb^{3+}(^7F_6) \longrightarrow Tb^{3+}(^5D_4) + Tb^{3+}(^7F_0).$$

As a result, the higher energy level emission ($^5D_3$) is quenched in favour of the lower energy level emission ($^5D_4$) giving rise to the strong green emission at about 544 nm.

This phenomenon can also be emphasized by the Fig. 8b where the peaks area ratio between $^5D_4 \rightarrow {}^7F_5$ and $^5D_3 \rightarrow {}^7F_6$ transition is studied upon UV excitation as a function of terbium concentration. Indeed, this ratio clearly increases when doping rate becomes higher than 0.4%Tb^{3+}. This study can not be achieved above 5% Tb^{3+} because emission arising from $^5D_3$ level vanishes.

In addition to the cross-relaxation phenomenon, a concentration quenching is also involved in the concentration dependence of YAG:Tb luminescence and hence greatly affects the emission properties. These two processes result in the existence of an optimal concentration for which luminescent properties are the most efficient [41, 47]. Relative yields, determined by integrating the area of the $^5D_4 \rightarrow {}^7F_5$ emission peak, are gathered in Fig. 9. The optimal Tb^{3+} concentration was estimated to be 20% ($x = 0.6$). Above it, concentration quenching dominates and emission intensity decreases.

Fig. 10 shows excitation spectra of the $^5D_4 \rightarrow {}^7F_5$ emission of Tb^{3+} (544 nm) in $Y^3Al^5O^{12}$:0.4%Tb^{3+} (a), $Y_3Al_5O_{12}$:5%Tb^{3+} (b) and $Y^3Al_5O_{12}$:20%Tb^{3+} (c). Several bands between 484 and 488 nm are discerned which may be assigned to the $^7F_6 \rightarrow {}_5D_4$ transition [48]. As the terbium concentration increases, a slight shift of the peak positions to higher energies is observed, due to the higher ionic radii of Tb^{3+} with respect to that of Y_{3+} ions. It is well known that the splittings decrease while increasing the ligand distance [49].

Decay time of the $^5D_4$ level was also examined by monitoring the $^5D_4 \rightarrow {}^7F_5$ emission located at 544 nm upon excitation at 485 nm. For all the samples investigated (Fig. 11), a single exponential decay is observed with a time constant mainly lying between 3 and 5 ms. Small increase of the $^5D_4$ lifetime is observed between $x = 0.012$ and $x = 0.3$, concentration for which the time constant reaches 4.5 ms. For higher concentrations, the shortening of the $^5D_4$ luminescence decay can be ascribed to energy tranfer between Tb^{3+} followed by partial trapping of the luminescence by unwanted impurities or defects. These results are in good agreement with previous studies on YAG:Tb [8, 50, 51].

4. Conclusion

Sol-gel route have been successfully used to prepare pure and Tb^{3+} doped-YAG powders. The crystallization temperature of the derived materials is much lower than that used in the conventional solid-state reaction, around 900°C instead 1500–1600°C, as indicated by XRD, TG/TDA and IR spectra. SEM results and ^{27}Al-NMR measurements allowed to characterize the powders morphology, which consists of large particles of narrow-size distribution, and the Al^{3+} local environment expected for YAG compounds.

For low Tb^{3+} contents, YAG material exhibit blue and green emission arising from $^5D_3$ and $^5D_4$ levels. Increase in the concentration leads to the extinction of that originating from $^5D_3$ by cross-relaxation mechanism, giving rise to strong fluorescence from $^5D_4$. The highest photoluminescence intensity from this level was observed with 20%Tb^{3+}.

Further work will be devoted to optical analysis upon VUV excitation since this material satisfies all the requirements to be an efficient VUV phosphor.

Acknowledgments

The authors would like to aknowledge Dr. Fabrice Leroux (CNRS) and Joël Cellier (University Clermont II) for many hours of helpful discussions concerning NMR and XRD measurements respectively.

References

1. A. IKESUE, T. KINOSHITA, K. KAMATA and K. YOSHIDA, *J. Am. Ceram. Soc.* **78** (1995) 1033.
2. S. SHIONOYA, in "Phosphor Hanbook" (CRC Press, Boca Raton, FL, 1998) p. 394 and p. 515.
3. G. BLASSE and A. BRIL, *Appl. Phys. Lett.* **11** (1967) 53.
4. K. OHNO and T. ABE, *J. Electrochem. Soc.* **133** (1986) 638.
5. *Idem., ibid.* **134** (1987) 2072.
6. R. P. RAO, in Proceedings of SPIE, Vol. **2651** (Liquid Crystal Materials, Devices, and Applications IV), San Jose, January–February 1996, edited by R. Shashidhar (SPIE, Washington, 1996) p. 139.
7. D. RAVICHANDRAN, R. ROY, A. G. CHAKHOVSKOI, C. E. HUNT, W. B. WHITE and S. ERDEI, *J. Lumin.* **71** (1997) 291.
8. C. H. PARK, S. J. PARK, B. Y. YU, H. S. BAE, C. H. KIM, C. H. PYUN and G. Y. HONG, *J. Mater. Sci. Lett.* **19** (2000) 335.
9. D. R. MESSIER and G. E. GAZZA, *Amer. Ceram. Soc. Bull.* **51** (1972) 692.
10. H. WANG, L. GAO and K. NIIHARA, *Mat. Sci. Eng. A* **288** (2000) 1.
11. T. CHEN, S. C. CHEN and C. YU, *J. Solid State Chem.* **144** (1999) 437.
12. X. LI, H. LIU, J. WANG, X. ZHANG and H. CUI, *Opt. Mater.* **25** (2004) 407.
13. Y. C. KANG, I. W. LENGGORO, S. B. PARK and K. OKUYAMA, *J. Phys. Chem. Solids* **60** (1999) 1855.
14. Y. HAKUTA, T. HAGANUMA, K. SUE, T. ADSCHIRI and K. ARAI, *Mat. Res. Bull.* **38** (2003) 1257.
15. Y. HAKUTA, K. SEINO, H. URA, T. ADSCHIRI, H. TAKIZAWA and K. ARAI, *J Mater. Chem.* **9** (1999) 2671.
16. G. GOWDA, *J. Mater. Sci. Lett.* **5** (1986) 1029.
17. Y. H. ZHOU, J. LIN, S. B. WANG and H. J. ZHANG, *Opt. Mater.* **20** (2002) 13.
18. Y. H. ZHOU, J. LIN, M. YU, S. M. HAN, S. B. WANG and H. J. ZHANG, *Mat. Res. Bull.* **38** (2003) 1289.
19. J. ZHANG, J. NING, X. LIU, Y. PAN and L. HUANG, *Mat. Res. Bull.* **38** (2003) 1249.
20. J. MCKITTRICK, K. KINSMAN, S. CONNELL, E. SLUZKY and K. HESSE in Ceramic Transactions, Vol. **26** (Forming Science and Technology for Ceramics), edited by M. J. Cima (The American Ceramic Society, Westville, OH, 1992) p. 17.
21. R. MANALERT and M. N. RAHAMAN, *J. Mater. Sci.* **31** (1996) 3453.
22. R. S. HAY, *J. Mater. Res.* **8** (1993) 578.
23. S.M. SIM, K.A. KELLER and T.I. MAH, *ibid.* **35** (2000) 713.
24. O. YAMAGUCHI, K. TAKEOKA and A. HAYASHIDA, *J. Mater. Sci. Lett.* **10** (1990) 101.
25. O. YAMAGUCHI, K. TAKEOKA, K. HIROTA, H. TAKANO and A. HAYASHIDA, *J. Mater. Sci.* **27** (1992) 1261.
26. M. VEITH, S. MATHUR, A. KAREIVA, M. JILAVI, M. ZIMMER and V. HUCH, *J. Mater. Chem.* **9** (1999) 3069.
27. S. K RUAN, J. G. ZHOU, A. M. ZHONG, J. F. DUAN, X. B. YANG and M. Z. SU, *J. Alloys Compounds* **275–277** (1998) 72.
28. D. BOYER, G. BERTRAND-CHADEYRON and R. MAHIOU, *Opt. Mater.* **26** (2004) 101.
29. D. BOYER, G. BERTRAND-CHADEYRON and R. MAHIOU, in Proceedings of SPIE, Vol. **5250** (Advances in Optical Thin Films), Saint-Etienne, France, Sept. 2003, edited by R. Shashidhar (SPIE, Washington, 2004) p. 286.
30. J. Y. CHOE, D. RAVICHANDRAN, S. M. BLOMQUIST, D. C. MORTON, K. W. KIRCHNER, M. H. ERVIN and U. LEE, *Appl. Phys. Lett.* **78** (2001) 3800.
31. J. R. LO, T. Y. TSENG, J. H. TYAN and C. M. HUANG, in Proceedings of the 9th International Vacuum Microelectronics Conference, St-Petersburg, Russia, December 1996 (Nevskii Kur'er, St-Petersburg, 1996) p. 197.
32. J. Y. CHOE, D. RAVICHANDRAN, S. M. BLOMQUIST, K. W. KIRCHNER, E. W. FORSYTHE and D. C. MORTON, *J. Lumin.* **93** (2001) 119.
33. G. CHADEYRON, R. MAHIOU, M. EL-GHOZZI, A. ARBUS, D. ZAMBON and J. C. COUSSEINS, *ibid.* **72–74** (1997) 564.

34. J. R. LO and T. Y. TSENG, *Mater. Chem. Phys.* **56** (1998) 56.
35. K. J. D MACKENZIE and T. KEMMITT, *Thermochim. Acta* **325** (1999) 13.
36. A. M. HOFMEISTER and K. R. CAMPBELL, *J. Appl. Phys.* **72** (1992) 638.
37. P. VAQUEIRO and M. A. LOPEZ-QUINTELA, *J. Mater. Chem.* **8** (1998) 161.
38. J. DONG and K. LU, *Phys. Rev. B* **43** (1991) 8808.
39. W. S. JUNG, S. AHN and D. KIM, *J. Mater. Chem* **8** (1998) 1869.
40. G. ENGELHARDT and D. MICHEL in "High Resolution Solid-state NMR of Silicates and Zeolites" (John Wiley & Sons, Chichester, 1987) p. 143.
41. W. F. VAN DER WEG, TH. J. A. POPMA and A. T. VINK, *J. Appl. Phys.* **57** (1985) 5450.
42. D. J. ROBBINS, B. COCKAYNE, B. LENT and J. L. GLASPER, *Solid State Commun.* **20** (1976) 673.
43. D. HRENIAK, W. STREK, P. MAZUR, R. PAZIK and M. ZABKOWSKA-WACLAWEK, *Opt. Mat.* **26** (2004) 117.
44. G. H. DIEKE and H. M. CROSSWHITE, *Appl. Opt.* **2** (1963) 675.
45. G. BLASSE and B. C. GRABMAIER, in "Luminescent Materials" (Springler-Verlag, Berlin, 1994) p. 44.
46. *Idem.*, in *ibid.* p. 100.
47. D. J. ROBBINS, B. COCKAYNE, B. LENT and J. L. GLASPER, *Solid State Commun.* **36** (1980) 691.
48. D. ZAKARIA, *PhD. Thesis*, Université Blaise Pascal, Aubière, France (1991) p. 80.
49. P. CARO, E. ANTIC, L. BEARING, O. BEAURY, J. DEROUET, M. FAUCHER, C. GUTTEL, O. K. MOUNE and P. PORCHER, in Proceedings of the "Colloque International du CNRS", Lyon, France, 1976 (Editions du CNRS, Paris, 1977) p. 71.
50. T. WELKER, *J. Lumin.* **48–49** (1991) 49.
51. J. P. VAN DER ZIEL, L. KOPF and L. G. VAN UITERT, *Phys. Rev. B* **6** (1972) 615.

Received 12 May 2004
and accepted 28 June 2005